Chapitre 4. Holocene climate history of the Nunatsiavut (northern Labrador, Canada) established from pollen and dinoflagellate cyst assemblages covering the past 7,000 years.

Résumé

Cette étude documente les dernièrs ~7000 ans d'histoire climatique de l'Holocène pour le Labrador et le Nunatsiavut en utilisant une séquence sédimentaire (812 cm) récupérée dans le fjord de Nachvak, le fjord le plus septentrionale du Nunatsiavut. En utilisant une approche multi-proxy combinant une solide chronologie AMS-^{14}C et les assemblages de fossiles de grains de pollen et les kystes de dinoflagellés (= dinokystes), nous avons pu comparer les enregistrements terrestres et marins dans le but d'obtenir une meilleure compréhension de l'évolution climatique de la fin de l'Holocène pour le Nunatsiavut. Les reconstitutions des conditions paléocéanographiques dans le fjord de Nachvak ont révélé une histoire climatique fortement influencée par l'océan Atlantique Nord et la mer du Labrador jusqu'à il y a 1000 ans. Depuis on observe une grande stabilité du climat de la région, probablement dû à un effet de barrière du courant du Labrador qui charrie les eaux froides de l'Arctique.

Abstract

This study documents the past ~7,000 years of Holocene climatic history for Labrador and Nunatsiavut, using a long sedimentary sequence (812 cm) retrieved in Nachvak fjord, one of the northernmost fjords of Nunatsiavut. Using a multi-proxy approach combining a solid AMS-^{14}C chronology and the fossil assemblages of pollen grains and dinoflagellate cysts (= dinocysts), we were able to compare the terrestrial and marine records in an effort to obtain a better understanding of the late Holocene climate history of the Nunatsiavut until the present-day. The reconstructions of the paleoceanographic conditions in Nachvak Fjord revealed a mid-late-Holocene climate history more strongly influenced by the North Atlantic Ocean and the Labrador Sea than the last 1,000 years of climate stability in the region, due to a barrier effect from cold Arctic waters of the Labrador Current.

4.1. Introduction

The climate history of the Holocene since the last deglaciation has been well documented in the Arctic, sub-Arctic, west and south Greenland and Newfoundland (Macpherson, 1982; Ritchie, 1987; Kaufman et al., 2004; Kerwin et al., 2004; Kaplan and Wolfe, 2006; Carlson et al., 2007; Renssen et al., 2009, Marcott et al., 2013). Labrador is the continental part of the province known as “Newfoundland and Labrador” on the northeastern Atlantic coast of Canada. Our study region is located in the northern part of the province that belongs to the native Labradorian Inuit also called the Nunatsiavut. Nachvak fjord is located in the Torngat Mountains National Park Reserve, hence it is a remote and pristine tundra ecosystem (Figure 4.1). The geographical, oceanographical and climatological characteristics of the region have been resumed in Richerol et al. (2012, 2014). The climate of Labrador is significantly influenced by the cold Labrador Current (Figure 4.1), resulting in a strong climatic contrast between the coastal and the interior Labrador (Engstrom and Hansen, 1985). In summer the mean temperature on the coast is 10°C while it can reach between 16-38°C inland. In winter the coast is relatively warmer than inland (Short and Nichols, 1977; Ullah et al., 1992). In the last decade, the Labrador fjords have been frozen from the second half of December to the first half of July (NCDC). The Nunatsiavut, and Labrador in general, have been known to be stable in terms of climate throughout the Industrial Era, with no evidence of fluctuations associated with the recent human-induced climate changes and the warming observed in most other Arctic and sub-Arctic regions (ACIA, 2005 ; Smol et al., 2005 ; IPCC, 2007 ; AMAP, 2011 ; Richerol et al., 2014). During the last glaciation (Wisconsinian : 85,000 to 10,000 BP), the Laurentide Ice Sheet covered the entire region. A warming period called the Holocene Thermal Maximum occurred 11,000 to 6,000 years ago. However, depending on the deglaciation pattern of the Laurentide Ice Sheet and the influence of orbital cycles, the timing and magnitude of the warming varied substantially between western and eastern Canada (Renssen et al., 2009). An abrupt deglaciation of the central part of the Laurentide Ice Sheet over Hudson Bay occurred between 9,000 and 8,400 BP due to glacial

outburst flood events through Hudson Strait (Barber et al., 1999; Dyke, 2004; Carlson et al., 2007; Lajeunesse and St-Onge, 2008). Paleoclimate records show a delayed onset of the Holocene Thermal Maximum between 7,000 and 6,000 BP over central and northeastern North America and southern Greenland (Kaufman et al., 2004; Kaplan and Wolfe, 2006; Carlson et al., 2007). In Newfoundland (South of Labrador), the deglaciation began around 10,000 BP and palynological records reveal that vegetation re-colonized the area after 9,300 BP (Macpherson, 1982; Ritchie, 1987; Shaw et al., 2002; Bell et al., 2005a; Shaw et al., 2006), allowing human settlement around the same period (Bell and Renouf, 2003; Bell et al., 2005b). Further North, around 7,000 BP, the conditions were cooler over regions directly influenced by the presence of the remnants of the Laurentide Ice Sheet (Bell and Renouf, 2003; Bell et al., 2005a, b; Renssen et al., 2009). Previous studies suggested its disappearance around 7,000 BP, with the persistence of some small ice caps in northern Québec and Labrador until 6,000 BP (Peltier, 2004; Carlson et al., 2008; Renssen et al., 2009; Saulnier-Talbot and Pienitz, 2010), delaying the recolonization by vegetation in Labrador to ~5,500-5,000 BP (Lamb, 1984, 1985). North of 56°N, Nunatsiavut (Figure 4.1) is a landscape of forest-tundra and tundra. In the forest tundra the most common tree species is the black spruce (*Picea mariana*) along with some white spruce (*Picea glauca*) and eastern larch (*Larix laricina*). The tundra is mostly composed of dwarf shrubs (*Betula papyrifera*, *B. glandulosa*, *Alnus crispa* and *Salix* spp.), graminoids, herbs, mosses and lichens (Lamb, 1984, 1985; Fallu et al., 2002; Roberts et al., 2006).

This study represents the first step in documenting the transitional period between the last glaciation and the Industrial Era for Labrador and Nunatsiavut. In 2009, a long sedimentary sequence (812 cm) was retrieved in Nachvak fjord, one of the northernmost fjords of Nunatsiavut (Figure 4.1). Our objectives were to use a multi-proxy approach in order to reconstruct part of the Holocene climate history within Nunatsiavut. Combining a solid AMS-^{14}C (Accelerator Mass Spectrometry) chronology and the fossil assemblages of pollen and dinocysts, we were able to

compare the terrestrial and marine records in an effort to obtain a better understanding of the mid-late Holocene climate history of the Nunatsiavut, from the beginning of interglacial conditions ~7,000 years ago until the present-day.

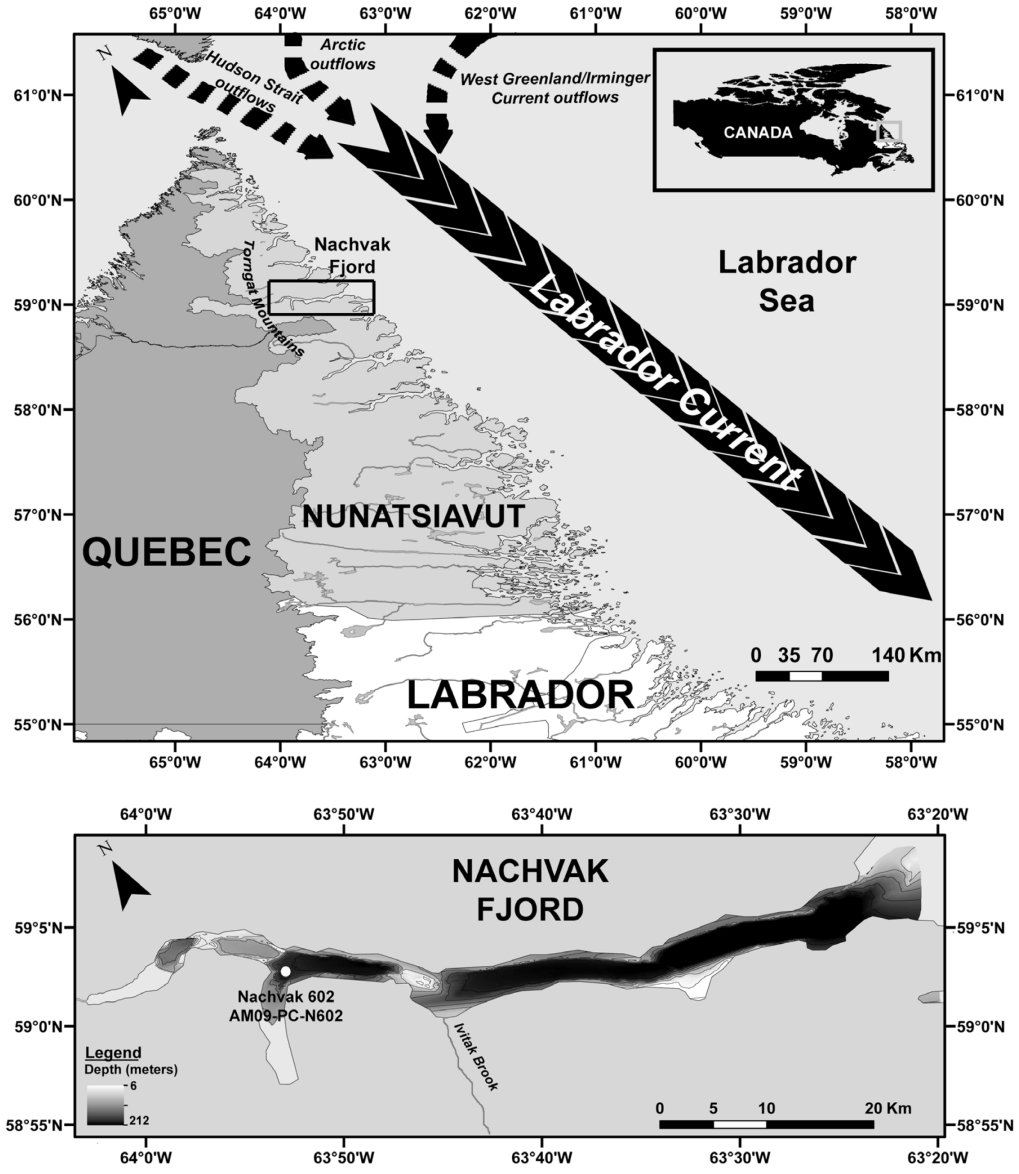

Figure 4.1 : Map of the Nunatsiavut (North Labrador, Canada) illustrating the location of the piston core retrieved from Nachvak fjord (modified from Richerol et al., 2012).

4.2. Methodology

4.2.1. Sampling

Sampling in Nachvak fjord was carried out in November 2009 during leg4b of the ArcticNet campaign onboard Canadian Coast Guard Ship Amundsen. A long sedimentary sequence (812 cm) was collected at station 602 (59.5265°N, 63.8784°W) using a piston corer triggered by a gravity corer. This piston-core was cut into eight sections of approximatively 100 cm each for easiest storage and transport. The eight sections were described and sampled at the Laboratory of Marine Palynology, ISMER-UQAR (Institut des sciences de la mer, Université du Québec à Rimouski), in Rimouski (Québec). The geophysical analyses (density, magnetic susceptibility) were performed at 0.5 cm intervals for each section. The percentages of organic matter and water content were measured every 1 cm. The grain-size and microfossil analyses (dinocysts, pollen and spores, *Halodinium* sp., foraminifer linings and pre-Quaternary palynomorphs) were performed at 10 cm intervals for each section in the Aquatic Paleoecology Laboratory (APL - Laval University, Quebec City). The palynological analyses were performed using the standard method described in Rochon et al. (1999) and Richerol et al. (2008a,b; 2012).

4.2.2. Stratigraphic analysis

Grain-size analysis

The particule-size composition of the core was determined at 10 cm intervals using the laser granulometer Horiba® LA950v2. The samples were prepared following the protocol from the Laboratory of Geomorphology and

Sedimentology at Laval University (Québec, QC). The free software Gradistat v4 (Blott and Pye, 2001) was used to statistically separate the different grain sizes and their percentages, as well as calculate standard statistical parameters (mean, median and sorting) using the mathematical “method of moments” (Krumbein and Pettijohn, 1938).

Multi-sensor core logger (MSCL)

Low-field volumetric magnetic susceptibility (K), density (d) and fractional porosity (FP) were measured at the Sedimentary Paleomagnetism and Marine Geology Laboratory of ISMER-UQAR (Rimouski, QC) using a GEOTEK™ MSCL at 0.5 cm intervals for each core.

The volumetric magnetic susceptibility (K) is a dimensionless parameter measuring the magnetisation of a volume induced by applying a magnetic field to a material. It is used for marine sediments because variations in density in sediment cores are relatively small (Gunn and Best, 1998). Because of the near zero magnetic susceptibility of the pore-water, the porosity can have an impact on the volumetric magnetic susceptibility by diluting the amount of magnetic carrier mineral in the core and thus underestimating the total magnetic susceptibility. We therefore quantified this effect (Kp) by assuming zero susceptibility for the pore volume (Niessen et al., 1998) :

$$Kp = K/(1-FP) \qquad [1]$$

4.2.3. Chronological framework

A chronology was established based on 20 AMS-^{14}C ages obtained from shell fragments found at various depths throughout the core. The preparation of the samples was performed at the Radiochronology Laboratory of the Center for Northern Studies (Laval University, Québec City, Canada) and the analyses at the

Keck Carbon Cycle AMS Facility (Earth System Science department, University of California at Irvine, USA). The calibration of conventional AMS-^{14}C dates into cal BP dates was done using the software CALIB 7.0 online (Stuiver et al., 2005) and MARINE13 (Reimer et al., 2013). The station 899 in Komaktorvik Fjord (Labrador: 59.28°N, -63.73°W), being the nearest of our coring site, was chosen to estimate a value for marine reservoir corrections (ΔR = 150 ± 40) (Table 4.1).

Table 4.1 : Table detailing the statistical data of the calibration of the AMS-^{14}C dates obtained throughout the core.

mean core depth (cm)	^{14}C age	95.4% (2σ) calibrated age ranges	relative area under distribution	cal BP*	calibration data
92.5	1505±15	cal BP 781-996	1.000	890±108	Reimer et al., 2013
148.5	2120±15	cal BP 1398-1646	1.000	1520±124	
212.5	2725±20	cal BP 2125-2341	1.000	2230±108	
347.5	3735±15	cal BP 3367-3586	1.000	3480±110	
407.5	4075±15	cal BP 3790-4062	1.000	3930±136	
411.5	4075±20	cal BP 3780-4062	1.000	3920±141	
433.5	4210±15	cal BP 3954-4232	1.000	4090±139	
444.5	4250±15	cal BP 3989-4289	1.000	4140±150	
448.5	4320±15	cal BP 4118-4393	1.000	4260±138	
458.5	4340±15	cal BP 4144-4403	1.000	4270±130	
464.5	4415±20	cal BP 4236-4505	1.000	4370±135	
473.5	4520±15	cal BP 4395-4653	0.992	4520±129	
		cal BP 4664-4675	0.008		
494.5	4700±20	cal BP 4605-4851	1.000	4730±123	
520.5	4865±15	cal BP 4825-5078	0.993	4950±127	
		cal BP 5100-5110	0.007		
556.5	5195±15	cal BP 5292-5517	1.000	5400±113	
630.5	5590±20	cal BP 5697-5913	1.000	5800±108	
636.5	5580±15	cal BP 5692-5904	1.000	5800±106	
647.5	5620±20	cal BP 5720-5943	1.000	5830±112	
804.5	6550±15	cal BP 6749-6993	1.000	6870±122	
810.5	6545±15	cal BP 6744-6987	1.000	6870±122	

** The authors of the Calib 7.0 software (Reimer et al., 2004, 2013) recommand to round the calibrated age ranges to the nearest 10 years for samples with standard deviations (± error in the age) greater than 50 years.*

4.2.4. Palynomorphs preparation

Fossil palynomorphs preparation (pollen, spores, dinocysts, acritarchs, freshwater and pre-Quaternary palynomorphs) followed standard procedures as outlined in Richerol et al. (2008a,b, 2012). Concentration of the palynomorphs (specimens cm^{-3}) was calculated.

Palynomorphs were counted using a transmitted-light microscope (Leica DM5500B) with a magnification factor of 400× at APL (UL, Quebec City). A minimum of 300 dinocysts were counted in each sample. This method yields the best statistical representation of all the taxa present in the samples. The nomenclature used for the identification of the dinocysts corresponds to Rochon et al. (1999), Head et al. (2001), the index of Lentin and Williams (Fensome and Williams 2004) and Radi et al. (2013). The identification of the pollen and spores was performed using the Laurentian flora of Frère Marie-Victorin (1935) as well as Rousseau (1974), to account for the species encountered in Nunatsiavut, and McAndrews et al. (1973) for the pollen and spores micrographs.

Studies from Zonneveld et al. (1997, 2001) and Zonneveld and Brummer (2000) have shown species sensitivity to oxygen availability. The cysts from the *Protoperidinium* group, such as *Brigantedinium* sp., are the most sensitive, followed by the genera *Spiniferites*, *Impagidinium* and *Operculodinium*. The high sedimentation rates measured in the Nunatsiavut fjords helped preserving dinocyst assemblages from oxidation (Richerol et al., 2014), and the most sensitive taxa, such as *Brigantedinium* spp., showed excellent preservation, with the operculum still attached on many specimens.

4.2.5. Statistical analyses

Biozonations through clustering

In order to statistically distinguish the major changes in the dinocyst and pollen assemblages, we used the R software in combination with the libraries “vegan” and “rioja” to produce a cluster showing the euclidean distance between each sample for each core. Using the “decostand” function, our relative abundance data have first been standardized prior to the transformation of the resultant data matrix to a euclidean distance matrix. The grouping test CONISS was then applied to the distance matrix using the “chclust” function (Borcard et al., 2011). For each core section, a graphical hierarchical clustering has been obtained according to time.

Pollen-based quantitative paleoclimatic reconstructions

The reconstructions of terrestrial environmental parameters were performed with the software “R” and the reconstruction technique of the modern analog (RecMAT). The modern pollen assemblage database includes ‘N = 4,833’ sites from lakes, peats, moss cushions, and other terrestrial deposits of North America and Greenland, distributed among 10 vegetation types (biomes) (Whitmore et al., 2005). The methodology applied has been described by Fréchette et al. (2008). We have chosen to group together the Asteraceae because of an inability to distinguish between different species. This database includes 69 climatic and bioclimatic parameters. The followings were reconstructed and results were compared with the dinocyst-based paleoceanographic reconstructions: mean monthly temperature (°C) and precipitation (mm) for each month, total annual precipitation (mm) and mean temperature of the coldest and warmest month (°C). The climate estimates were calculated from the five best modern analogues. The validation of the database provided strong correlation coefficients and a RMSE (Root Mean Square Error) for each reconstructed parameter (Table 4.2).

Table 4.2 : Table summarizing the information on the parameters reconstructed from assemblages of fossil pollen and dinocyst (from Richerol et al., 2014) : parameter denomination and codename, unit, coefficient de correlation (R^2) and Root Mean Square Error (RMSE) of the validation.

Parameter	Unit	R^2	±RMSE
Pollen-based paleoclimatic reconstructions			
Total Annual Precipitation	mm	0.81	210.35
Mean Temperature of the Coldest Month of the year	°C	0.92	3.26
Mean Temperature of the Warmest Month of the year	°C	0.91	1.67
Dinocyst-based paleoceanographic reconstructions (Richerol et al., 2014)			
Sea-surface Temperature of August	°C	0.95	1.72
Sea-surface Salinity of August	psu	0.72	2.22
Sea-ice Cover Duration	months $year^{-1}$	0.86	1.33
Annual Productivity	g C m^{-2} $year^{-1}$	0.80	61.27

Dinocyst-based quantitative paleoceanographic reconstructions

The reconstructions of sea-surface parameters were performed with the software “R” using fossil dinocyst assemblages, transfer functions and the search of five analogs in the GEOTOP modern dinocyst database (N = 1,441) (Richerol et al., 2008b, 2014). Here we also used the "bioindic" package developed on the R-platform (http://cran.r-project.org/), which is specially designed to offer various types of statistical analyses.

4.3. Results

4.3.1. Chronological framework

The 20 AMS-^{14}C dates obtained (Table 4.1) do not show any reworking of sediments and a fitting curve extrapolates a $R^2 = 0.9884$. The time span represented by the core covers the last ~7,000 BP. The calibrated dates yield a mean sedimentation rate of 0.1176 cm year^{-1} with a bottom date at 6,870 ± 122 cal BP. The last 2,000 years are represented in the upper 175 cm of the core (Figure 4.2).

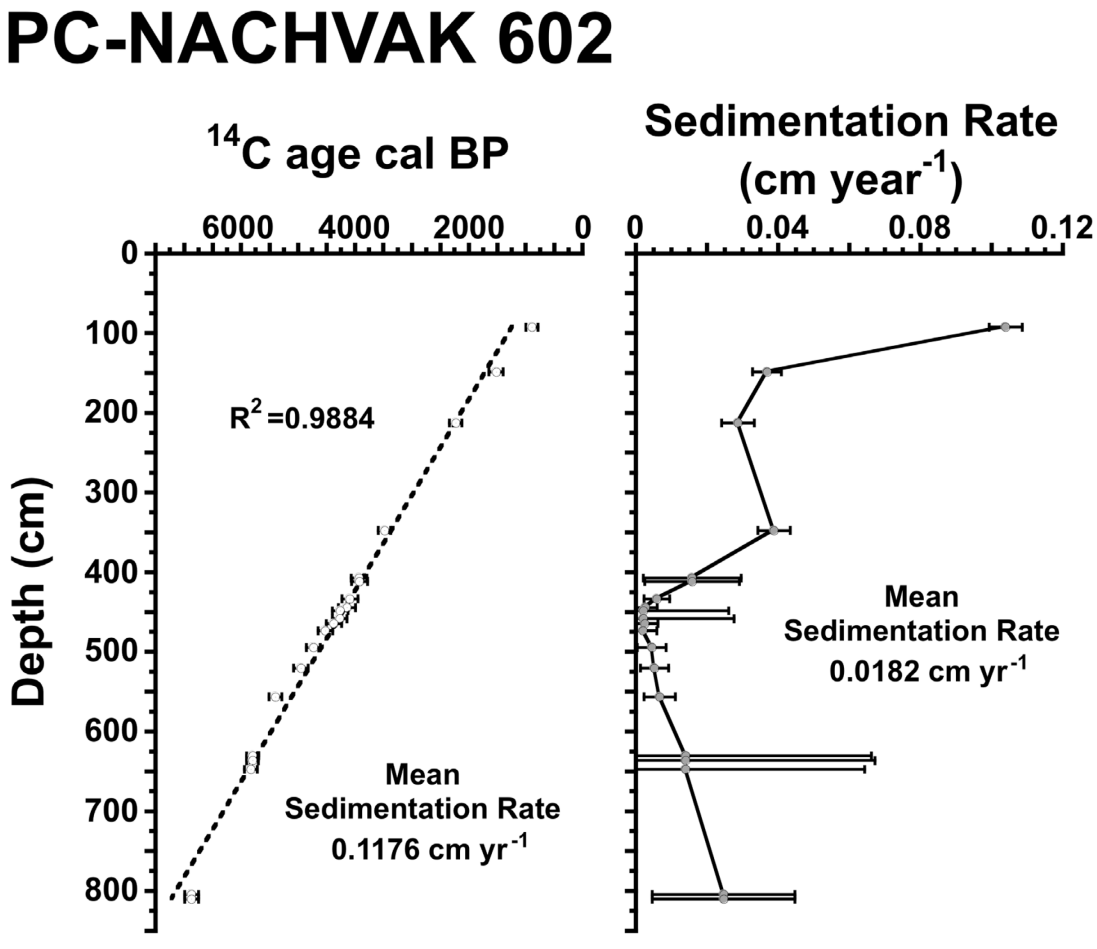

Figure 4.2 : Age-depth model based on the AMS-^{14}C chronology from the piston core.

4.3.2. Sedimentology

Sediments generally showed a polymodal grain size distribution and were "*moderately well sorted*" to "*very poorly sorted*" (Krumbein and Pettijohn, 1938; Blott and Pye, 2001) (Figure 4.3).

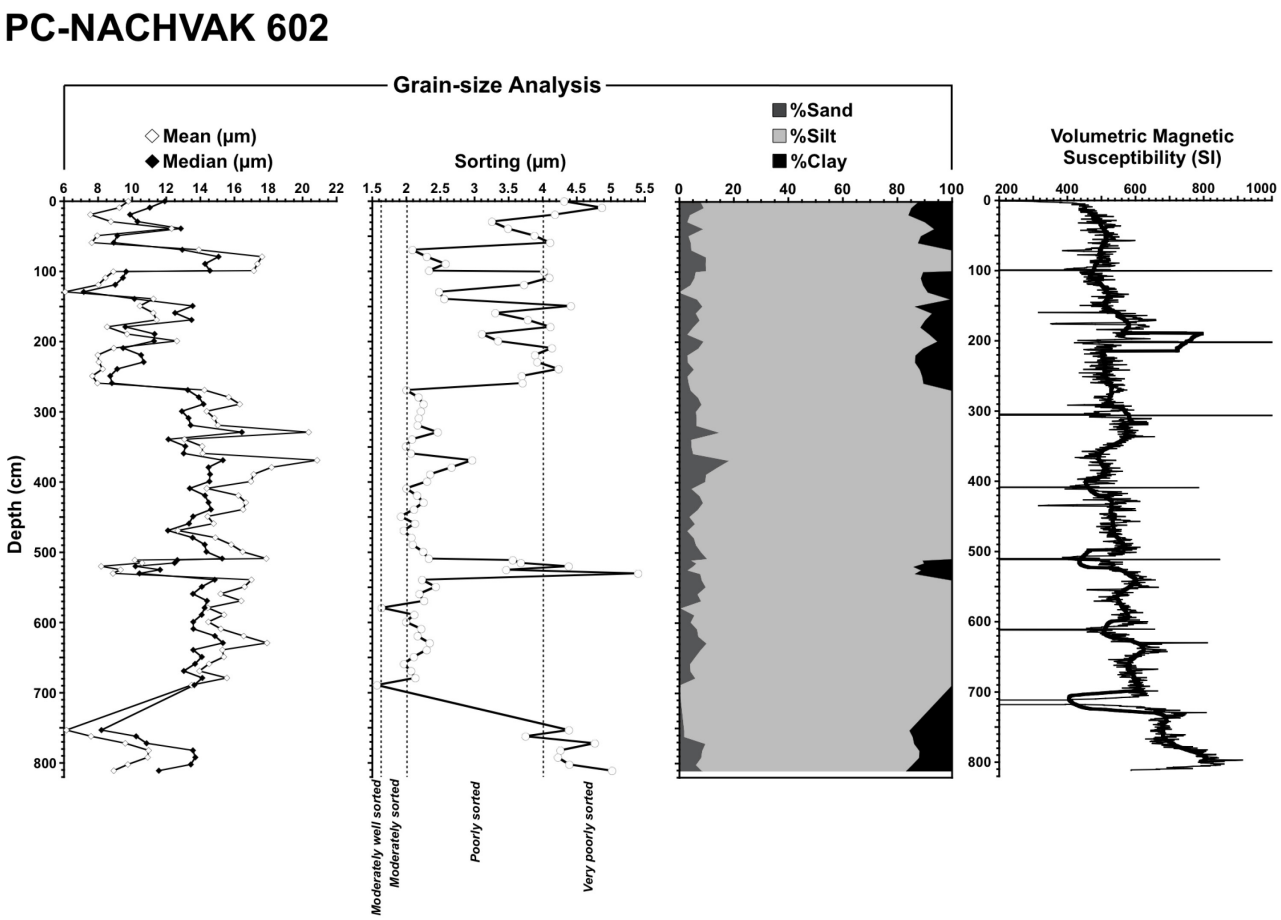

Figure 4.3 : Sedimentological analyses of the core represented on a depth scale (cm). From left to right: grain-size analysis (mean, median and sorting (µm)), percentages of silt and sand, and volumetric magnetic susceptibility corrected for fractional porosity (SI).

We observed a dominant silt fraction (> 60%), a clay fraction (< 20%) and a sand fraction (mostly < 10%). With the exception of a peak of 20% between 540-510 cm (5,200-4,800 cal BP), the clay fraction disappeared between ~700-280 cm (~6,000-2,800 cal BP). In the same interval, mean and median reached their highest values, and the sorting is lowest. Moreover, the mean is strongly superior to the median, illustrating a more coarsely skewed distribution (i.e., more fine than coarse material) (Bouchard et al., 2011). Mean and median grain sizes were correlated with silt and clay percentages (the finer particles), whereas sorting profiles coincided with sand percentages (the coarser particles) (Bouchard et al., 2011).

Once corrected for the porosity, the volumetric magnetic susceptibility showed a general decreasing trend from bottom to top, from ~840 SI to ~240 SI. Some peaks appear at regular interval along the core; these are artefacts from the ends of the 1 m-long sections of the piston core (Figure 4.3). Between the base of the core and ~730 cm downcore, the decrease is faster (~240 SI), while between ~730 cm and the top of the core the volumetric magnetic susceptibility decrease is slow, remaining mostly between ~400 and ~600 SI. In the uppermost ~5 cm, the volumetric magnetic susceptibility decreased from ~400 to ~240 SI (Figure 4.3).

4.3.3. Palynomorph fluxes

In addition to the dinocysts, which are good indicators of planktonic productivity (Richerol et al., 2008b), we have identified and counted four other types of palynomorphs (Figure 4.4):

- *Halodinium* sp., an acritarch and freshwater tracer (Richerol et al., 2008b);

- the terrestrial palynomorphs such as pollen grains and spores, which allow comparing terrestrial and marine climate changes (Richerol et al., 2008b);

- the foraminifer linings, indicators of benthic marine productivity (de Vernal et al., 1992);

- the pre-Quaternary palynomorphs (reworked palynomorphs), including dinocysts, acritarchs, pollen grains and spores, which are indicators of inputs of ancient and/or distant erosive material (de Vernal et Hillaire-Marcel, 1987; Durantou et al., 2012).

Using the sedimentation rates (cm $year^{-1}$) calculated and extrapolated from the AMS-^{14}C analyses and palynomorph concentration (specimen cm^{-3}), we were able to calculate fluxes of these palynomorphs in specimens cm^{-2} $year^{-1}$ (Figure 4.4).

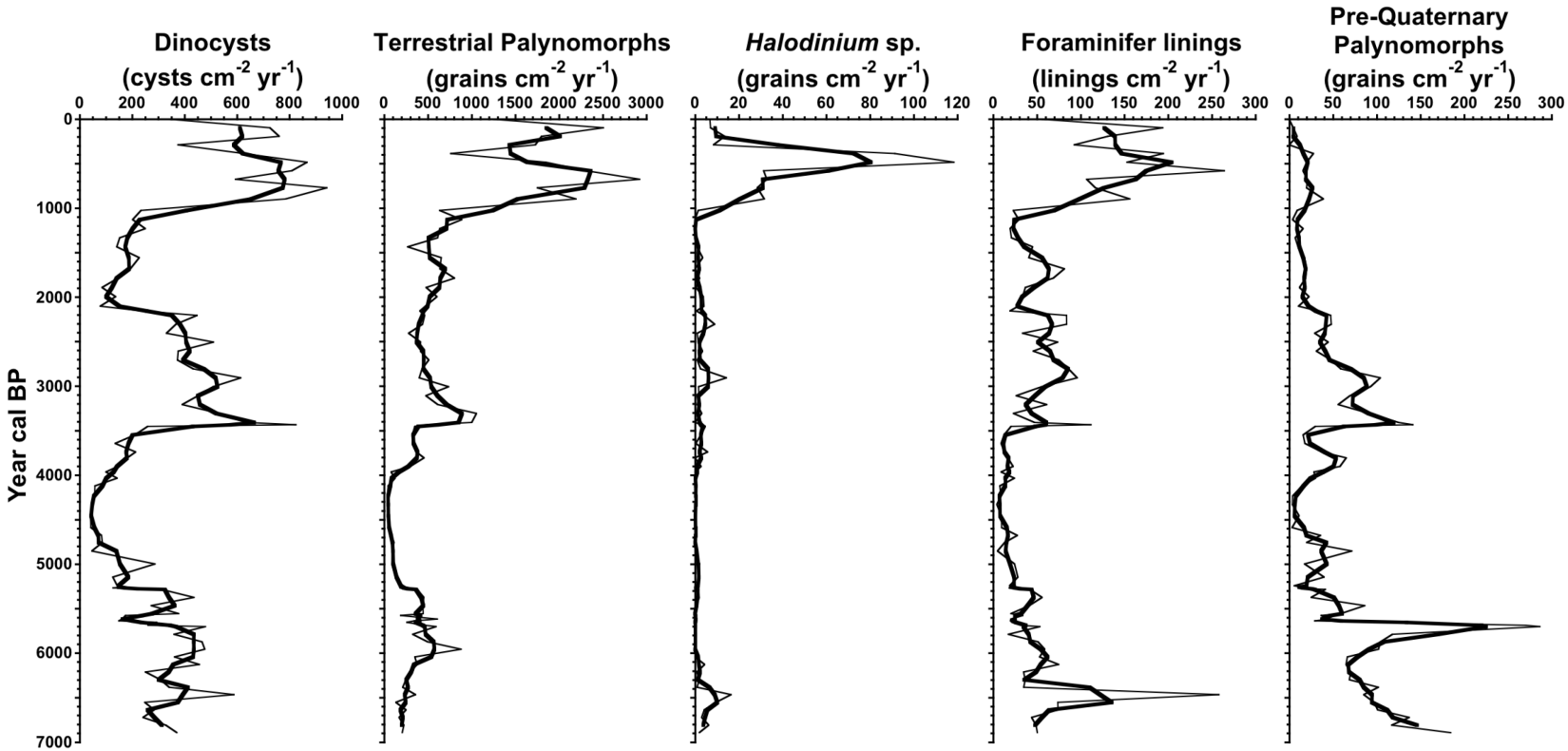

Figure 4.4 : Fluxes of the five types of palynomorphs counted, according to time (year cal BP): dinocyst (cysts cm^{-2} $year^{-1}$), terrestrial palynomorphs (grains cm^{-2} $year^{-1}$), *Halodinium* sp. (grains cm^{-2} $year^{-1}$), foraminifer linings (linings cm^{-2} $year^{-1}$) and pre-Quaternary palynomorphs (grains cm^{-2} $year^{-1}$). For each curve, the black thick line is a smooth on three values.

All palynomorphs show similar trends throughout the length of the core and display a series of oscillations between high and low flux values (Figure 4.4). High values of all palynomorphs occur between ~7,000-5,200 cal BP, ~3,600-2,100 cal BP and ~1,000-700 cal BP. During the first interval, pre-Quaternary palynomorphs reach their maximum value at 285 grains cm^{-2} yr^{-1}. During the last period, all palynomorphs, with the exception of pre-Quaternary palynomorphs, reach their maximun values: dinocyst fluxes 1,000 grains cm^{-2} yr^{-1}, terrestrial palynomorphs 3,000 grains cm^{-2} yr^{-1}, *Halodinium* 120 grains cm^{-2} yr^{-1} and foraminifer linings 270 grains cm^{-2} yr^{-1}. Minimum values of all palynomorphs occur between 5,200-3,600 cal BP and a decreasing trend is observed from 700 cal BP until today.

4.3.4. Pollen and Spore Assemblages

The core assemblages portray a type of vegetation linked to tundra and forest-tundra landscapes (Lamb, 1984; Fallu et al., 2002; Roberts et al., 2006), with a strong abundance of shrub-like trees pollen (*Betula* sp. and *Alnus crispa*), a relatively high abundance of coniferous trees pollen (*Pinus* sp. and *Picea* sp.) with some herbs pollen (Cyperaceae, Chenopodiaceae, Ericaceae, Asteraceae, *Epilobium latifolium*) and spores (Figure 4.5).

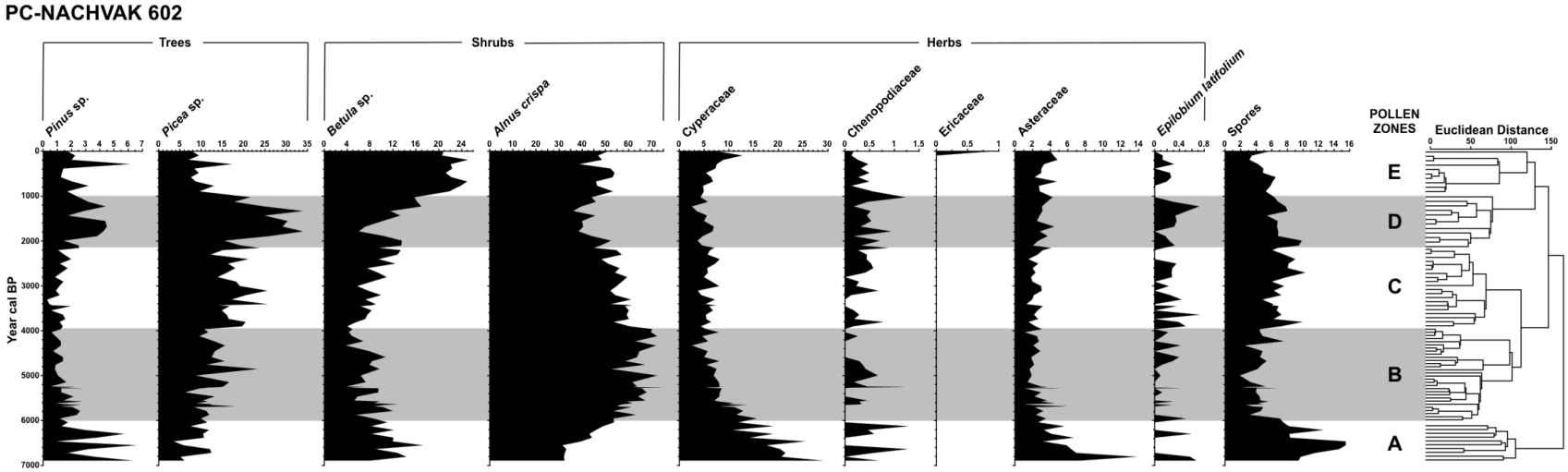

Figure 4.5 : Pollen and spore zones identified based on the relative abundances (%) of major species observed in the core, according to time (year cal BP). Different shades of gray represent pollen zones obtained for each core using a cluster analysis.

Five pollen zones can be distinguished. Zone A, at the bottom of the core between 7,000-6,000 cal BP, is characterised by the lowest relative abundances of *A. crispa* (on average 38%) and the shrub-like tree pollen grains (on average 50%) and the highest abundances of herbs pollen (on average 27%) of the whole core. From 6,500 to 6,000 cal BP there is a notable increase in *A. crispa* pollen abundance (+20%) concomittant to a decrease in herbs pollen grains (-15%).

Zone B, between 6,000-4,000 cal BP, is mainly characterised by the maximum abundance of *A. crispa* (on average 63%) and the dominance of the shrub-like tree pollen (on average 71%). We also observed a drop of the abundance of herbs pollen to its present proportions (on average between 9-11%).

Zone C, between 4,000-2,000 cal BP, is characterised by an increase in the relative abundance of coniferous trees pollen (+5%), especially *Picea* sp. We also observed an equivalent decrease of the relative abundance of the shrub-like trees pollen (-6%), especially *A. crispa*.

Zone D, between 2,000-1,000 cal BP, is characterised by the highest abundance of coniferous trees pollen grains (on average 28%) and another drop of 10% in the relative abundance of the shrub-like trees pollen.

Zone E (the last 1,000 cal BP) is characterised by the highest abundance of *Betula* sp. (on average 22%) and the dominance of shrub-like trees pollen (on average 71%). The relative abundance of the coniferous trees pollen decreased to the level of zone A.

4.3.5. Dinocyst Assemblages

The sediment core is characterised by the dominance of dinocysts belonging to heterotrophic taxa of dinoflagellates (*Islandinium minutum* s.l., *Brigantedinium* spp., *Echinidinium karaense* and *Polykrikos* Arctic Morphotypes I

and II). Only one dinocyst species associated with autotrophic dinoflagellate taxa is present (*Pentapharsodinium dalei*). It has a high abundance (on average 55%) between 7,000-3,400 cal BP and disappears around ~2,600 cal BP (Figure 4.6).

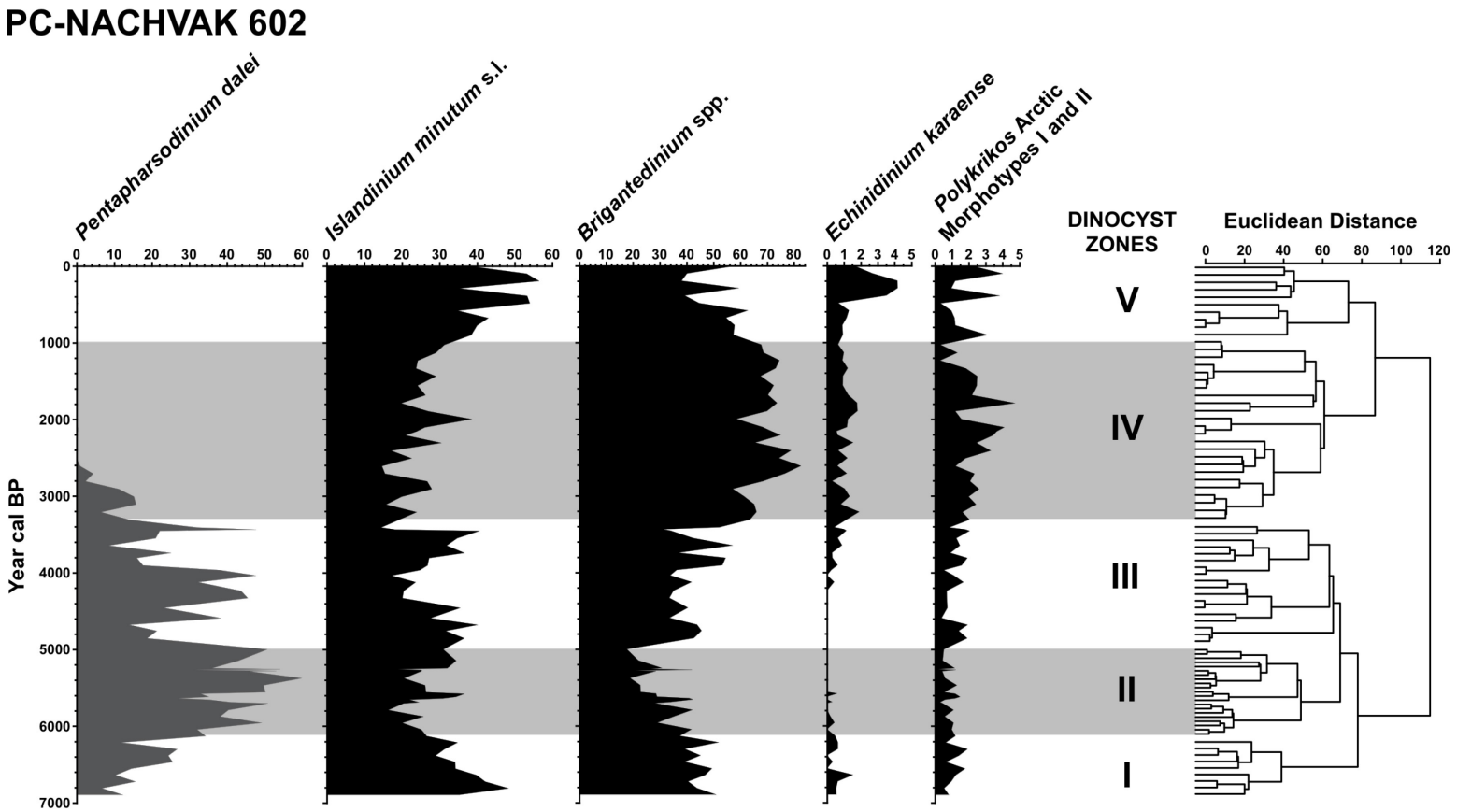

Figure 4.6 : Dinocyst zones identified based on the relative abundances (%) of major species observed in the core, according to time (year cal BP). Different shades of gray represent pollen zones obtained for each core using a cluster analysis.

We identified five main dinocyst zones. Zone I, between 7,000-6,200 cal BP, is characterised by the dominance of heterotrophic (on average 83%) over autotrophic (on average 16%) taxa. In this interval we observe the concurrent increase of *P. dalei* (on average +20%) and decrease of *I. minutum* s.l. and *Brigantedinium* spp. (on average -20%).

Zone II, between 6,200-5,000 cal BP, is characterised by the highest abundance of *P. dalei* (on average 42%) and the lowest abundance of heterotrophic taxa (on average 58%).

Zone III, between 5,000-3,200 cal BP, is characterised by the steady decrease of *P. dalei* (on average -14%) and the concurrent increase of the heterotrophic taxa (on average +13%).

Zone IV, between 3,200-1,000 cal BP, is characterised by the final disappearance of *P. dalei* at the beginning of the period (between 3,310-2,709 cal BP) and the highest abundance of *Brigantedinium* spp. (on average 70%) and *Polykrikos* Arctic Morphotype I and II (on average 2%). This zone marks also the appearance of *E. karaense*.

Zone V, the last 1,000 cal BP, is characterised by the total dominance of the heterotrophic taxa with the highest abundance of *I. minutum* s.l. (on average 45%) and *E. karaense* (on average 2%).

4.3.6. Paleoclimatic reconstructions

Pollen-based reconstructions

Using the modern analogs chosen for the pollen-based reconstructions, their origin and frequency of occurrence, we were able to document which type of biome

have influenced the region over the last ~7,000 years. A graphic representation presents the average monthly temperature and precipitation for each pollen zone (Figure 4.7).

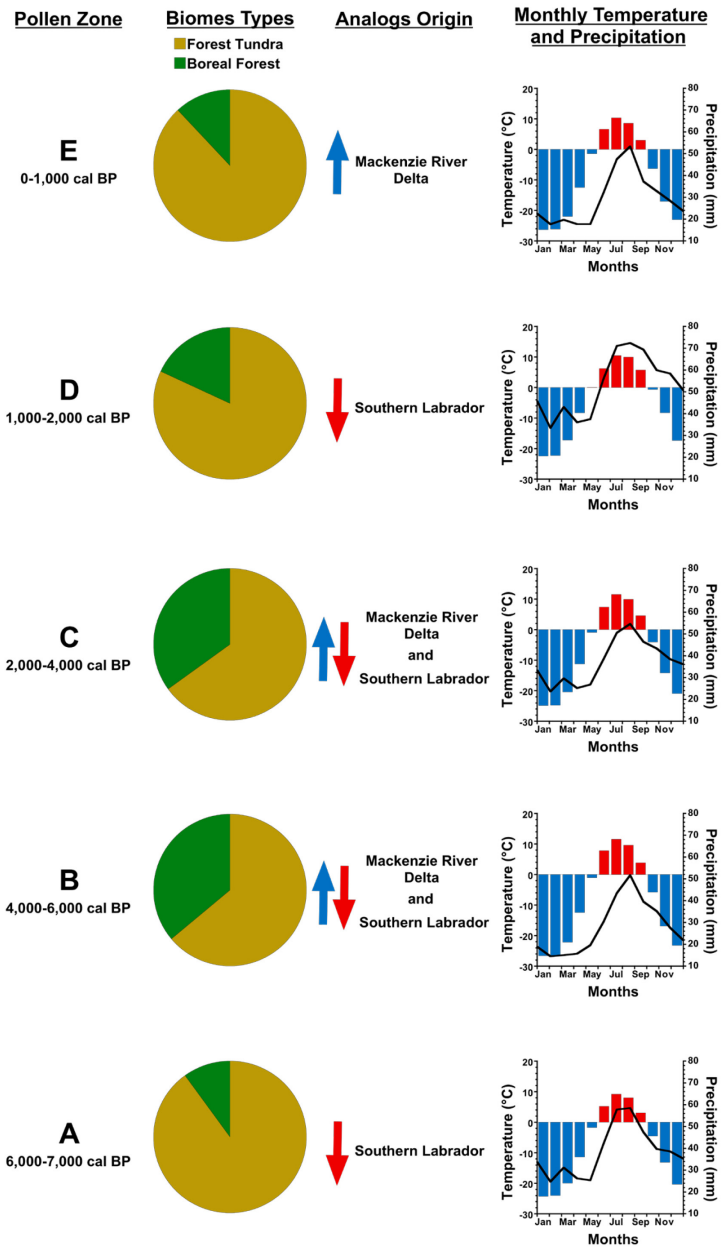

Figure 4.7 : Graphic representation, according to the five pollen zones, of the biomes types and origin of the analogs, and the mean monthly temperature (°C – the bars) and precipitation (mm – the line). The blue up arrow illustrate the cold northern origin of the analogs, and the red down arrow their warmer southern origin.

Over the considered time period, the region was mostly influenced by "Forest Tundra" biomes. The analogs chosen in pollen zone A came mostly from sites in southern Labrador, suggesting warmer conditions. The strongest influence of the "Boreal Forest" biomes was inferred for the period 6,000-2,000 cal BP (zones B and C) associated with analogs from sites "colder" (Mackenzie River Delta) and "warmer" (Southern Labrador). The paleoclimatic reconstructions show dryer summers and slightly cooler winters. Zone D marks the decrease of the "Boreal Forest" influence, associated with dryer and warmer winters and the wettest summers (Figure 4.7). The last ~1,000 years show dominance of the "Forest Tundra" influence over the region, with colder winters and dryer summers, and analogs mostly from "colder" sites (Figure 4.7).

The three other reconstructed parameters show two types of trends. First, the annual precipitation and the mean temperature of the coldest month follow the same pattern of variation (Figure 4.8). A more or less important decrease between ~7,000-6,000 cal BP (-200 mm and -2°C, respectively), followed by stable conditions between ~6,000-2,000 cal BP (~320 mm and -27°C, respectively) only disrupted by two peaks at ~3,800 cal BP (+200 mm and +3°C respectively) and ~3,100 cal BP (+300 mm and +4°C respectively) (Figure 4.8). Then an important increase occurs between ~2,000-1,000 cal BP (+400 mm and +5°C respectively), followed by a decrease in the last ~1,000 years (-400 mm and -5°C respectively) (Figure 4.8). The third reconstructed parameter, the mean temperature of the warmest month, shows a very different trend. First, we observe an increase between ~7,000-6,000 cal BP (+4°C), followed by a very stable trend until present-day (around 10°C) (Figure 4.8).

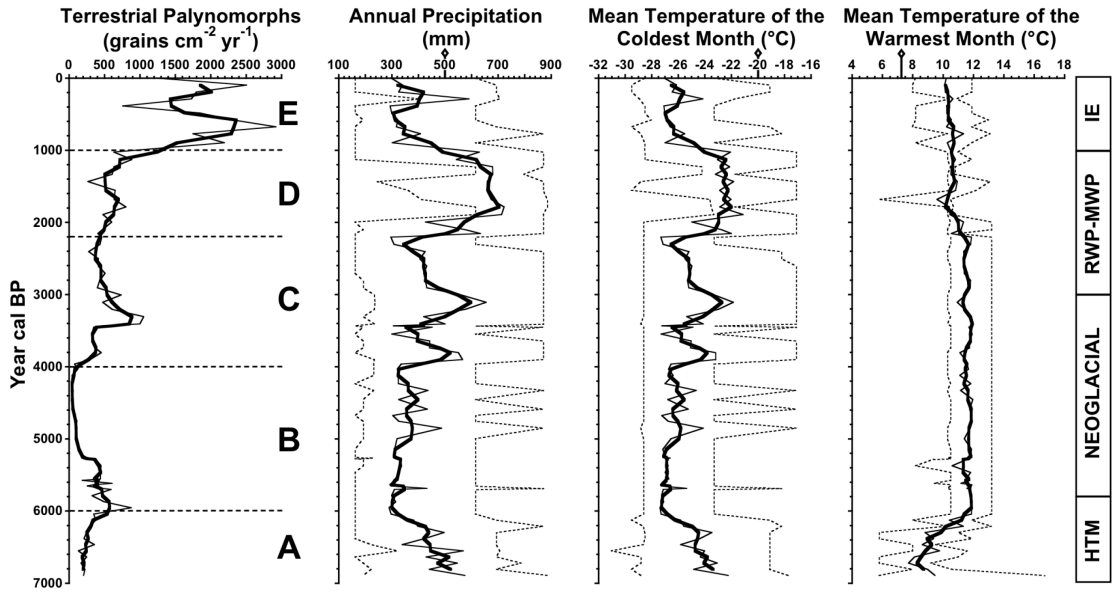

Figure 4.8 : Evolution of terrestrial palynomorph fluxes (grains cm^{-2} $year^{-1}$) in parallel with three reconstructed terrestrial parameters, according to time (year cal BP) : Annual Precipitation (mm) and Mean Temperature of the Coldest and Warmest Month (°C). For each curve, the black thick line is a smooth on three values. Horizontal black dotted lines on terrestrial palynomorphs fluxes represent major shift in pollen zones. Vertical dotted lines represent the confidence interval for each reconstructed parameter over time. For each parameter, the black empty diamonds on the x-axis represent modern values estimated from nearby meteorological stations (Cartwright 57°W and Goose A 60°W (Environment Canada)). HTM = Holocene Thermal Maximum; RWP = Roman Warm Period; MWP = Medieval Warm Period; IE = Industrial Era.

Dinocyst-based reconstructions

The reconstructions of sea surface parameters are generally in good agreement with the measured modern values of the environmental conditions (Richerol et al., 2012) (Figure 4.9).

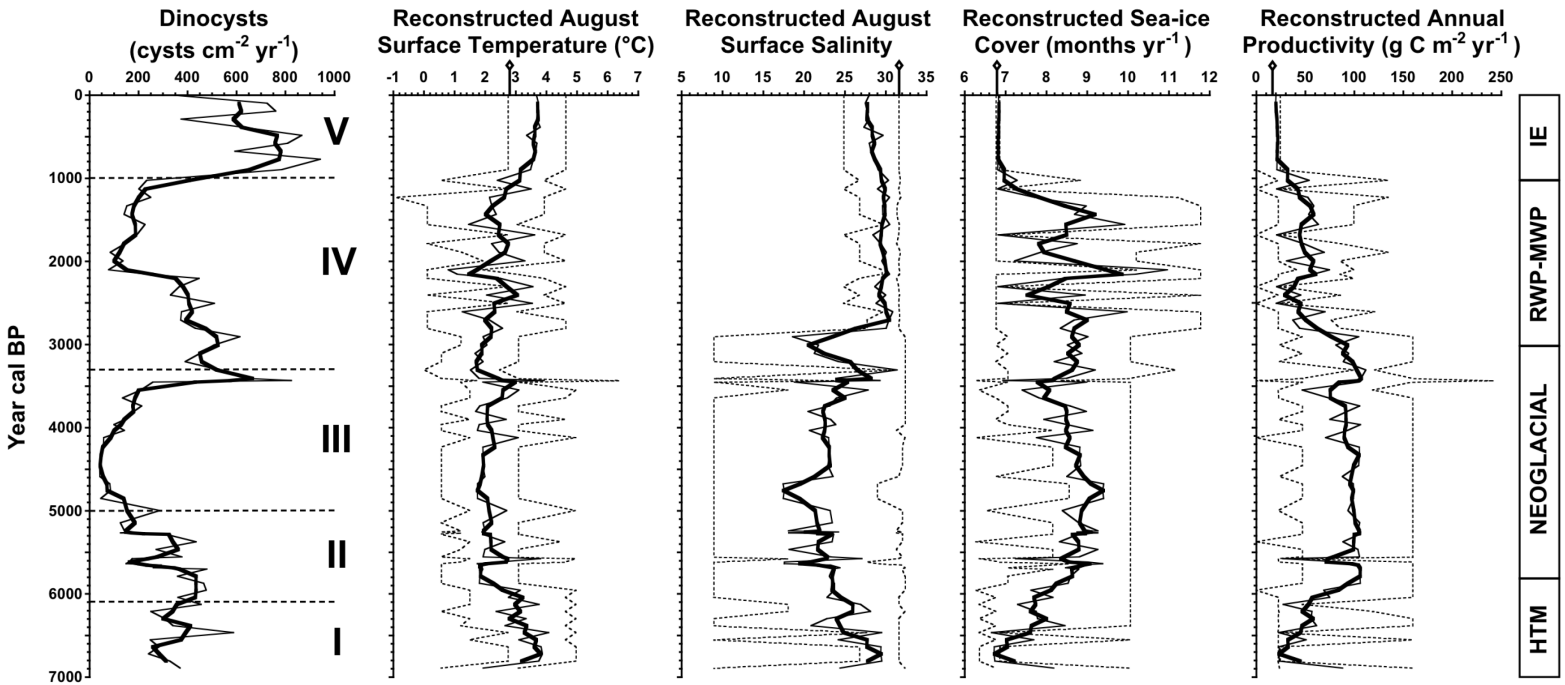

Figure 4.9 : Evolution of dinocyst fluxes (cysts cm^{-2} $year^{-1}$) in parallel with the four reconstructed oceanographic parameters, according to time (year cal BP) : August Sea-Surface Temperature (°C), August Sea-Surface Salinity, Sea-Ice Cover duration (months $year^{-1}$) and Annual Productivity (g C m^{-2} $year^{-1}$). For each curve, the black thick line is a smooth on three values. Horizontal black dotted lines on dinocyst fluxes represent major shift in dinocyst zones. Vertical dotted lines represent the confidence interval for each reconstructed parameter over time. For each parameter, the black empty diamonds on the x-axis represent modern values. HTM = Holocene Thermal Maximum; RWP = Roman Warm Period; MWP = Medieval Warm Period; IE = Industrial Era.

Between ~7,000-5,800 cal BP, the reconstructed sea-surface temperatures for the warmest month of the year (August) declined by ~2°C, reaching temperatures comparable to the modern values. Meanwhile, the reconstructed sea-surface salinity for the warmest month decreased by ~6 units, whereas the reconstructed sea-ice cover duration and annual productivity increased by ~2 months $year^{-1}$ and ~80 g C m^{-2} $year^{-1}$, respectively (Figure 4.9).

Between ~5,800-3,000 cal BP, the reconstructed August temperatures remained stable around ~2°C, with the exception of a peak at ~3°C between ~3,800-3,300 cal BP. The reconstructed salinity remained stable around ~22, with the exception of an abrupt decrease to 17 at ~4,800 cal BP and a peak at 28 between 3,700-3,000 cal BP. The reconstructed sea-ice cover duration remained stable around ~8.6 months $year^{-1}$, with the exception of a peak to ~9.4 months $year^{-1}$ at ~4,800 cal BP and a decrease to ~7.6 months $year^{-1}$ between 3,800-3,300 cal BP. The reconstructed annual productivity remained stable around ~100 g C m^{-2} $year^{-1}$, with the exception of a decrease to ~60 g C m^{-2} $year^{-1}$ at ~5,600 cal BP and another one to ~70 g C m^{-2} $year^{-1}$ between ~4,200-3,500 cal BP (Figure 4.9).

Between ~3,000-1,000 cal BP, reconstructed temperature generally showed an increasing trend (+1.2°C) with variations of the order of 1.4 to 3°C. In this interval, the salinity sharply increases from 19 to 29 (its modern value) within 300 years. The reconstructed sea-ice cover duration showed a decreasing trend (-2 months $year^{-1}$) with important variations between ~10 and ~7 months $year^{-1}$. The reconstructed annual ocean productivity showed a decreasing trend of -60 g C m^{-2} $year^{-1}$ over the period (Figure 4.9). Over the last ~1,000 years, the four reconstructed parameters remained relatively stable within the range of their modern instrumental values (Figure 4.9).

4.4. Discussion

This study describes features of the mid-late Holocene paleoclimate variability in the Labrador area, yet with slight deviations in the timing when compared to climate patterns reported from other Arctic and Subarctic regions (Peltier, 2004; Carlson et al., 2008; Renssen et al., 2009). Based on the AMS-^{14}C chronology, our paleorecord goes back in time to approximately ~7,000 cal BP corresponding to the end of the Holocene Thermal Maximum in northern Labrador (Kaufman et al., 2004; Kaplan and Wolfe, 2006; Carlson et al., 2007) (Figure 4.2, Table 4.1).

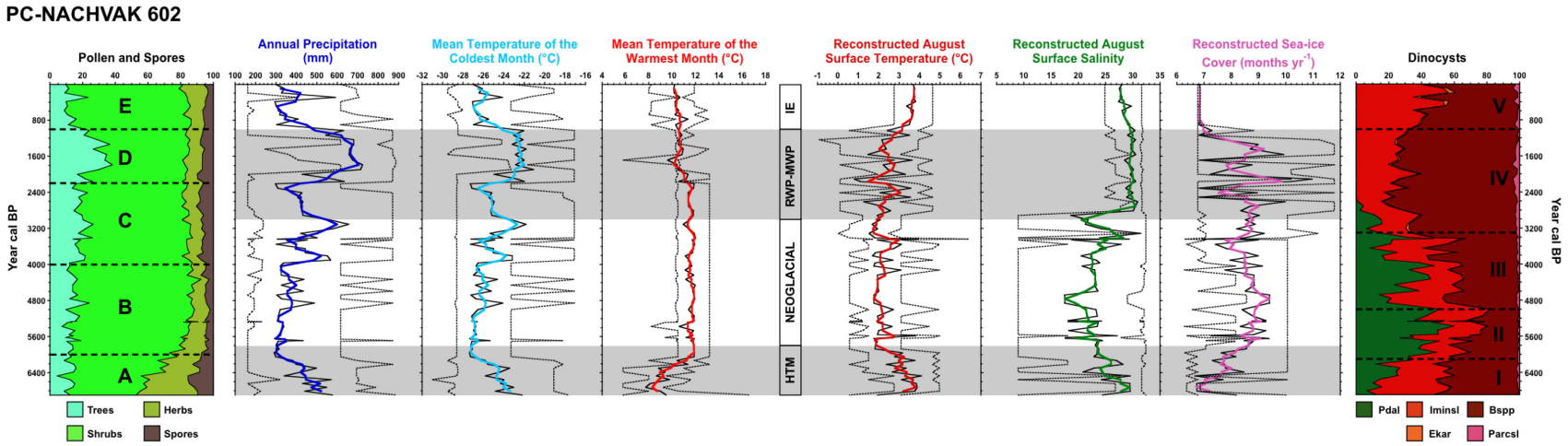

Figure 4.10 : Synthesis of the information gathered from fossil pollen and dinocyst assemblages in relation to time (year cal BP). Left side of the figure: relative abundance (%) of pollen of trees, shrub-like trees, herbs and spores, annual precipitation (mm) and mean temperature of the coldest and warmest months (°C). Right side of the figure: relative abundances (%) of major species of dinocysts observed, August sea-surface temperature (°C) and salinity, and sea-ice cover duration (months year^{-1}). Horizontal black dotted lines on abundance graphs represent major shifts in pollen and dinocyst assemblage zones. Vertical dotted lines represent the confidence interval for each reconstructed parameter through time. HTM = Holocene Thermal Maximum; RWP = Roman Warm Period; MWP = Medieval Warm Period; IE = Industrial Era.

4.4.1. Holocene Thermal Maximum (HTM) – 5,800-7,000 cal BP

The higher volumetric magnetic susceptibility values recorded at the bottom of the core (810-720 cm; ~7,000-6,000 cal BP) (Figure 4.3), together with the higher flux of pre-Quaternary palynomorphs during approximately the same period (~7,000-5,600 cal BP) (Figure 4.4), suggest important detrital matter inputs, which can be associated with high meltwater influx from the remaining Laurentide Ice Sheet at the end of the last deglaciation (Peltier, 2004; Carlson et al., 2008). During the same period, palynomorph fluxes show a peak in *Halodinium* sp. and foraminifer linings, which can be linked to freshwater inputs and an increase of the benthic productivity (Figure 4.4). Considering the similar shifts in the fluxes of dinocysts and terrestrial palynomorphs all along the core, they portray synchronous variations in both terrestrial and marine habitats (Figure 4.4). Pollen zone A (7,000-6,000 cal BP) shows a relatively high abundance of herbaceous taxa consistent with recently deglaciated landscapes and the recolonization by terrestrial vegetation (Figures 4.5 and 4.10) (Richard, 1981; Ritchie, 1987; Viau and Gajewski, 2009; Jessen et al., 2011). Dinocyst zone I (7,000-6,200 cal BP) shows an increase in *P. dalei* and a decrease of *I. minutum* s.l., suggesting an increase in productivity and a decrease of cold Arctic water intrusions (Figures 4.6 and 4.10). The climatic parameters reconstructed with the pollen assemblage show a decrease of the temperature of the coldest month associated with an increase of the warmest month (Figures 4.8 and 4.10). These events can be interpreted as a return to conditions with a stronger seasonality after a glacial era. The marine reconstructions suggest a slight cooling trend, together with a decrease in salinity and longer sea-ice duration (Figures 4.9 and 4.10) coherent with colder and dryer winter conditions on land (Figures 4.7, 4.8, 4.10) and consistent with the end of deglaciation, input of freshwaters from the melting Laurentide Ice Sheet and the onset of the next cooling period, the Neoglacial (Figures 4.8, 4.9, 4.10) (Levac and de Vernal, 1997; Seidenkrantz et al., 2008; Nørgaard-Pedersen and Mikkelsen, 2009; Jessen et al., 2011; Solignac et al., 2011).

4.4.2. Neoglacial – 5,800-3,200 cal BP

The onset of the Neoglacial was dated at ~3,200 BP in southern and southwestern Greenland (Seidenkrantz et al., 2008), but at ~4,800 BP in Ikersuaq fjord and Narsaq Sound in southern Greenland (Nørgaard-Pedersen and Mikkelsen, 2009). Solignac et al. (2011) showed colder sea-surface conditions North and South of Newfoundland between ~5,700-4,000 BP thereby suggesting an earlier onset of the Neoglacial. A previous study of modern and fossil (the last ~200-300 years) dinocyst assemblages in Nachvak Fjord has shown the absence of *P. dalei* and proposed a stronger influence of Arctic waters than in the southernmost fjords of the region (Richerol et al., 2014). Rochon and de Vernal (1994) have associated *P. dalei* with the assemblage characteristic of the Labrador Sea and distinct from the assemblage of the Labrador shore and Labrador Current, similar to those inside the Labrador fjords. The presence of *P. dalei* between ~7,000-2,600 cal BP could be a signal of Labrador Sea water intrusions and of North Atlantic influences inside the fjord (Figures 4.6 and 4.10). The grain-size analysis shows a change in the sorting of the sediments between ~5,200-4,800 cal BP (Figure 4.3), corresponding to a slight increase in pre-Quaternary palynomorph fluxes between 5,300-4,700 cal BP (Figure 4.4). Pollen zone B (~6,000-4,000 cal BP) shows an important abundance of *A. crispa*, associated with tundra type vegetation and cold conditions (Figure 4.5). Although the modern pollen analogs show an increasing influence of warmer “Boreal Forest” type biomes and occurrence of southern Labrador sites, the influence of colder “Forest Tundra” type biomes is dominant (Figure 4.7). Richard (1981) documented the growth of Forest Tundra in Nunavik (Northern Québec) over the same period, suggesting cold terrestrial conditions. Dinocyst zones II and III (~6,000-3,300 cal BP) show a high abundance of *P. dalei* and an increase in the abundance of *I. minutum* s.l., suggesting high productivity and a higher input of cold Arctic waters, respectively (Figures 4.6 and 4.10). Our reconstructions also suggest colder conditions in Nunatsiavut starting around ~6,000 cal BP

(Figures 4.8, 4.9, 4.10). The grain-size analysis and the pre-Quaternary palynomorph fluxes seem to have registered an input of distant erosive material into the fjord. Previous studies suggested the influence of the melting glaciers from the Canadian Arctic and Greenland (Fisher et al., 1995; Vinther et al., 2009; Solignac et al., 2011), which could explain the inferred low salinities and higher productivity associated with the presence of *P. dalei* between ~6,000-3,000 cal BP (Figures 4.6, 4.9, 4.10). Both pollen and dinocysts have recorded between ~5,800-3,200 cal BP a cold period in Nunatsiavut (Figure 4.10). The paleoceanographic reconstructions suggest a growing cooling influence of Labrador Sea and North Atlantic waters over this period.

The sea-surface conditions northeast of Newfoundland have shown less severe conditions after ~4,000 BP, which could reflect a general decrease in cold water export through the Labrador Current linked to colder conditions in the Arctic resulting in decreased ice melt (Solignac et al., 2011). Pollen zone C (~4,000-2,000 cal BP) is similar to pollen zone B in term of analogs (Figure 4.7) and shows an increase of *Picea* sp. and a decrease of *A. crispa* (Figure 4.5), suggesting more pollen transport from Boreal Forest and a slight warming of the terrestrial conditions. The pollen reconstructions for this period show two peaks of warmer and wetter conditions at 3,800 cal BP and 3,100 cal BP (Figures 4.8 and 4.10). Dinocsyt zone III (~5,000-3,300 cal BP) shows a disappearance trend of *P. dalei* and an increase of *I. minutum* s.l. and *Brigantedinium* spp. (Figures 4.6 and 4.10). The marine reconstructions for this period show cold and stable conditions with a slight warming trend until 3,500 cal BP when a peak in temperature appears (Figures 4.9 and 4.10). During this period, an important decrease in salinity is mirrored by an increase in sea-ice cover duration (Figures 4.9 and 4.10). The lower salinity could indirectly reflect the wetter continental conditions and increased input of freshwater into the fjord, while *Halodininium* sp. shows a slight increase during this period (Figure 4.4) and the pollen reconstructions reveal a slight increase in the mean monthly precipitation between pollen zones B and C (Figure 4.8). The

resulting input of freshwater could also be responsible for the slight warming of the surface waters in the fjord.

4.4.3. Roman Warm Period-Medieval Warm Period (RWP-MWP) – 3,200-1,000 cal BP

The paleoclimatic reconstructions obtained with the last 1,000 years of pollen zone C (3,200-2,200 cal BP) suggest terrestrial conditions more in line with the end of the Neoglacial than the RWP-MWP (Figures 4.8 and 4.10). By comparing them to the paleoceanographic reconstructions, we observe a lag of 1,000 years in the transition between both periods (Figure 4.10). The RWP-MWP seems to have begun later (around 2,000 cal BP) on land.

Pollen zone D (~2,000-1,000 cal BP) shows the highest *Picea* sp. abundances (Figures 4.5). Mostly, the modern pollen analogs came from site in southern Labrador, but show less influence from “Boreal Forest” type biome (Figure 4.7), suggesting an opening of the vegetation cover and a bias toward tree pollen. The paleoclimatic reconstructions show warmer and wetter conditions (Figure 4.8 and 4.10). This period corresponds to the second half of the dinocyst zone IV, with the total disappearance of *P. dalei* and the maximum abundance of *Brigantedinium* spp. (Figures 4.6 and 4.10). The marine reconstructions show fluctuations in the sea-surface temperature and sea-ice cover between ~3,000-1,400 cal BP, and a stabilization of the salinity around its modern value. Between 1,400-1,000 cal BP, the temperature increase and the sea-ice cover duration decrease to their modern values (Figures 4.9 and 4.10). This warming trend, recorded both by the pollen and the dinocysts between 3,000-1,000 cal BP, is likely associated with both the Roman Warm Period (~2,000-1,500 cal BP) and the Medieval Warm Period (~1,300-900 cal BP) (Seidenkrantz et al., 2008; Solignac et al., 2011; Moros et al., 2012). The disappearance of *P. dalei* marks the end of the influence of the Labrador Sea and North Atlantic.

4.4.4. Industrial Era (IE) – the last 1,000 cal BP

In the northern hemisphere, the last ~1,000 years are usually marked by the colder period of the Little Ice Age (~500-200 BP) and the warming of the Industrial Era (the last ~200 years) (Seidenkrantz et al., 2008; Nørgaard-Pedersen and Mikkelsen, 2009; Solignac et al., 2011; Moros et al., 2012). The Labrador Sea region is known to have shown some discrepancies with regard to this scheme of paleoclimatic record. Most of the studies completed in the area do not show signs of the warming associated with the Industrial Era but instead reveal very stable climatic conditions with even a slight cooling trend (Laing et al., 2002; Viau and Gajewski, 2009; Richerol et al.,2014). In this study, pollen zone E reflects the establishment of the modern-day conditions of the fjords with a dominance of *Betula* sp. and *A. crispa* (Richerol et al., 2014), which are characteristic of shrub tundra vegetation and cooler conditions (Figures 4.5 and 4.10). Meanwhile, dinocyst zone V indicates the same scenario for the marine realm, with an increase in *I. minutum* s.l. and *E. karaense* usually associated with cold Arctic waters of the Labrador Current (Figures 4.6 and 4.10). The marine reconstructions show stable paleoceanographic conditions for the four parameters over the same period (Figures 4.9 and 4.10).

4.5. Conclusions

By combining geophysical and palynological data from a pristine fjord environment in northern Labrador, our study has provided new insights into the late Holocene climate history of the Nunatsiavut region over the last ~7,000 years. While Nachvak Fjord is mostly under Arctic Water influence, the presence of *P. dalei* illustrated a period of higher productivity and stronger influence from the Labrador Sea and North Atlantic inside the fjord between ~7,000-3,000 cal BP.

The last ~1,000 years of paleoceanographic history did not show any of the climate fluctuations usually associated with the cooling of the Little Ice Age or the warming associated with the Industrial Era. The absence of *P. dalei* during this period illustrates a stronger influence of the cold Labrador Current in the fjord system, acting as a barrier against the influence of the Labrador Sea and North Atlantic waters. This entire period appears to have remained climatically stable in this region as documented in previous studies.

Our study shows that, despite the modern climate stability of the region with regards to the climate changes, its past climate history has nevertheless revealed the sensitivity of the fjord systems as recorders of important climatic shifts, both local and regional, in the North Atlantic region. It thus confirms the importance of the Nunatsiavut fjords as sentinels for a better understanding of the complete past climate variability of the Northern Hemisphere, for the purpose of rendering more reliable predictions of future climate trajectories for this region.

Acknowledgements

This work was funded through grants from the Natural Sciences and Engineering Research Council of Canada (NSERC) and the Network of Centers of Excellence program ArcticNet awarded to Reinhard Pienitz and André Rochon, as well as through funding from the Nunatsiavut Government. The Center for Northern Studies (CEN) provided additional logistic support. We wish to thank the officers and crew of the CCGS Amundsen for their help and support during the sampling at sea.

References

Arctic Climate Impact Assessment (ACIA), 2005. International Arctic Science Committee (IASC), Cambridge University Press, 1020 pp.

Arctic Monitoring and Assessment Programme (AMAP), 2011. Snow, Water, Ice and Permafrost in the Arctic (SWIPA): Climate Change and the Cryosphere. AMAP, Oslo, Norway. 538 pp.

Barber, D. C., Dyke, A., Hillaire-Marcel, C., Jennings, A. E., Andrews, J. T., Kerwin, M. W., Bilodeau, G., MacNeely, R., Southon, J., Morehead, M. D. and Gagnon, J.-M., 1999. Forcing of the cold event of 8,200 years ago by catastrophic drainage of Laurentide lakes. Nature, 400, 344-348.

Bell, T. and Renouf, M. A. P., 2003. Prehistoric cultures, reconstructed coasts : Maritime Archaic Indian site distribution in Newfoundland. World Archaeology, 35(3), 350-370.

Bell, T., Daly, J., Batterson, M. J., Liverman, D. G. E., Shaw, J. and Smith, I. R., 2005a. Late Quaternary relative sea-level change on the West coast of Newfoundland. Géographie physique et Quaternaire, 59(2-3), 129-140.

Bell, T., Macpherson, J. B. and Renouf, M. A. P., 2005b. Late Prehistoric Human impact on Bass Pond, Port au Choix. Newfoundland and Labrador Studies, 20(1), 12pp.

Blott, S. and Pye, K., 2001. GRADISTAT: a grain size distribution and statistics package for the analysis of unconsolidated sediments. Earth Surface Processes and Landforms, 26(11), 1237-1248.

Borcard, D., Gillet, F. and Legendre, P., 2011. Numerical Ecology with R : Chapter 4 – Cluster Analysis. Gentleman, R., Hornik, K. and Parmigiani, G. G. (Eds), Use R! Series, Springer, New-York.

Carlson, A. E., Clark, P. U., Raisbeck, G. M. and Brook, E. J., 2007. Rapid Holocene deglaciation of the Labrador sector of the Laurentide Ice Sheet. Journal of Climate, 20, 5126-5133.

Carlson, A. E., Legrande, A. N., Oppo, D. W., Came, R. E., Schmidt, G. A., Anslow, F. S., Licciardi, J. M. and Obbink, E. A., 2008. Rapid early Holocene deglaciation of the Laurentide ice sheet. Nature Geoscience, 1, 620-624.

de Vernal, A. et Hillaire-Marcel, C., 1987. Paléoenvironnements du Wisconsinien moyen dans l'est du Canada par l'analyse palynologique et isotopique de sédiments océaniques et continentaux. Revue de Géologie Dynamique et de Géographie Physique, 27, 119-130.

de Vernal, A., Bilodeau, G., Hillaire-Marcel, C. and Kassou, N., 1992. Quantitative assessment of carbonate dissolution in marine sediments from foraminifer linings vs. shell ratios; Davis Strait, Northwest North Atlantic. Geology, 20(6), 527-530.

Durantou, L., Rochon, A., Ledu, D., Schmidt, S. and Babin, M., 2012. Quantitative reconstruction of sea-surface conditions over the last ~150 yr in the Beaufort Sea based on dinoflagellate cyst assemblages: the role of large-scale atmospheric circulation patterns. Biogeosciences, 9, 5391-5406.

Dyke, A. S., 2004. An outline of North American Deglaciation with emphasis on central and northern Canada. In Ehlers, J. and Gibbard, P. L. (Eds): Quaternary Glaciations – Extent and Chronology, Part II: North America, Vol. 2b. Elsevier Science and Technology Books, 373-424.

Engstrom, D. R., Hansen, B. C. S., 1985. Postglacial vegetational change and soil development in southeastern Labrador as inferred from pollen and chemical stratigraphy. Canadian Journal of Botany 63, 543-561.

Fallu, M.-A., Allaire, N. and R. Pienitz, 2002. Distribution of freshwater diatoms in 64 Labrador (Canada) lakes: species-environment relationship along latitudinal

gradients and reconstruction models for water colour and alkalinity. Canadian Journal of Fisheries and Aquatic Sciences, 59(2), 329-349.
Fensome, R.A. and Williams, G.L., 2004. The Lentin and Williams index of fossil dinoflagellages. Contribution Series Number 42, American Association of Stratigraphic Palynologists Foundation, Dallas, TX.
Fisher, D. A., Koerner, R. M. and Reeh, N., 1995. Holocene climatic records from Agassiz Ice Cap, Ellesmere Island, NWT, Canada. The Holocene, 5, 19-24.
Fréchette, B., de Vernal, A., Guiot, J., Wolfe, A.P., Miller, G. H., Fredskild, B., Kerwin, M. W. and Richard, P. J. H., 2008. Methodological basis for quantitative reconstruction of air temperature and sunshine from pollen assemblages in Arctic Canada and Greenland. Quaternary Science Reviews, 27, 1197–1216.
Frère Marie-Victorin, É. C., 1935. Flore Laurentienne. Les Presses de l'Université de Montréal, Montréal (QC) Canada.
Head, M.J., Harland, R. and Matthiessen, J., 2001. Cold marine indicators of the late Quaternary : the new dinoflagellate cyst genus Islandinium and related morphotypes. Journal of Quaternary Science, 16(7), 621-636.
Intergovernmental Panel on Climate Change (IPCC), 2007. World Meteorological Organisation, Cambridge University Press.
Jessen, C. A., Solignac, S., Nørgaard-Pedersen, N., Mikkelsen, N., Kuijpers, A. and Seidenkrantz, M.-S., 2011. Exotic pollen as an indicator of variable atmospheric circulation over the Labrador Sea region during the mid to late Holocene. Journal of Quaternary Science, 26(3), 286-296.
Kaplan, M. R. and Wolfe, A. P., 2006. Spatial and temporal variability of Holocene temperature in the North Atlantic region. Quaternary Research, 65, 223-231.
Kaufman, D. S., Ager, T. A., Anderson, N. J., Anderson, P. M., Andrews, J. T., Bartlein, P. J., Brubaker, L. B., Coats, L. L., Cwynar, L. C., Duvall, M. L., Dyke, A. S., Edwards, M. E., Eisner, W. R., Gajewski, K., Geirsdóttir, A., Hu, F. S., Jennings, A. E., Kaplan, M. R., Kerwin, M. W., Lozhkin, A. V., MacDonald, G. M., Miller, G. H., Mock, C. J., Oswald, W. W., Otto-Bliesner, B. L., Porinchu, D. F., Rühland, K., Smol, J. P., Steig, E. J. and Wolfe, B. B., 2004. Holocene thermal maximum in the western Arctic (0-180°W). Quaternary Science Review, 23, 529-560.
Kerwin, M. W., Overpeck, J. T., Webb, R. S. and Anderson, K. H., 2004. Pollen-based summer temperature reconstructions for the eastern Canadian boreal forest, subarctic, and Arctic. Quaternary Science Reviews, 23, 1901-1924.
Laing, T. E., R. Pienitz and S. Payette, 2002. Evaluation of limnological responses to recent environmental change and caribou activity in the riviere George region, Northern Québec, Canada. Arctic, Antarctic and Alpine Research, 34(4), 454-464.
Lamb, H. F., 1984. Modern pollen spectra from Labrador and their use in reconstructing Holocene vegetational history. Journal of Ecology, 72(1), 37-59.
Lamb, H. F., 1985. Palynological evidence for postglacial change in the position of tree limit in Labrador. Ecological Monographs, 55(2), 241-258.
Lajeunesse, P. and St-Onge, G., 2008. The subglacial origin of the Lake Agassiz-Ojibway final outburst flood. Nature Geoscience, 1, 184-188.
Levac, E. and de Vernal, A., 1997. Postglacial changes of terrestrial and marine environments along the Labrador coast: palynological evidence from cores 91-045-005 and 91-045-006, Cartwright Saddle. Canadian Journal of Earth Sciences, 34, 1358-1365.
Macpherson, J. B., 1982. Postglacial vegetational history of the eastern Avalon Peninsula, Newfoundland, and Holocene climatic change along the Eastern Canadian seaboard. Géographie Physique et Quaternaire, 36, 175-196.

Marcott, S. A., Shakun, J. D., Clark, P. U. and Mix, A. C., 2013. A reconstruction of regional and global temperature for the past 11,300 years. Science, 339, 1198-1201.
McAndrews, J.H., Berti, A. A. and Norris, G., 1973. Key to the Quaternary pollen and spores of the Great Lakes region. Royal Ontario Museum, Toronto, 65pp.
Moros, M., Jansen, E., Oppo, D. W., Giraudeau, J. and Kuijpers, A., 2012. Reconstruction of the late-Holocene changes in the Sub-Arctic Front position at the Reykjanes Ridge, north Atlantic. The Holocene, 22(8), 877-886.
Nørgaard-Pedersen, N. and Mikkelsen, N., 2009. 8000 year marine record of climate variability and fjord dynamics from Southern Greenland. Marine Geology, 264, 177-189.
Peltier, W., 2004. Global glacial isostasy and the surface of the ice-age Earth: the ICE-5G (VM2) model and GRACE. Annual Review of Earth and Planetary Sciences, 32, 111-149.
Radi, T., Bonnet, S., Cormier, M.-A., de Vernal, A., Durantou, L., Faubert, E., Head, M. J., Henry, M., Pospelova, V., Rochon, A. and Van Nieuwenhove, N., 2013. Operational taxonomy and (paleo-)autoecology of round, brown, spiny dinoflagellate cysts from the Quaternary of high northern latitudes. Marine Micropaleontology, 98, 41-57.
Reimer, P. J., Bard, E., Bayliss, A., Beck, J. W., Blackwell, P. G., Ramsey, C. B., Buck, C. E., Cheng, H., Edwards, R. L., Friedrich, M., Grootes, P. M., Guilderson, T. P., Haflidason, H., Hajdas, I., Hatté, C., Heaton, T., Hoffmann, D., Hogg, A. G., Hughen, K. A., Kaiser, K. F., Kromer, B., Manning, S. W., Niu, M., Reimer, R. W., Richards, D. A., Scott, E. M., Southon, J. R., Staff, R. A., Turney, C. S. M. and van der Plicht, J., 2013. INTCAL13 and MARINE13 radiocarbon age calibration curves 0-50,000 years cal BP. Radiocarbon, 55(4), 1869-1887.
Renssen, H., Seppä, H., Heiri, O., Roche, D. M., Goosse, H. and Fichelet, T., 2009. The spatial and temporal complexity of the Holocene thermal maximum. Nature Geoscience, 2, 411-414.
Richard, P. J. H., 1981. Paléophytogéographie postglaciaire en Ungava par l'analyse pollinique. Paléo-Québec, 13, 153pp.
Richerol, T., Rochon, A., Blasco, S., Scott, D. B., Schell, T. M. and Bennett, R. J., 2008a. Distribution of dinoflagellate cysts in surface sediments of the Mackenzie Shelf and Amundsen Gulf, Beaufort Sea (Canada). Journal of Marine Systems, 74, 825-839.
Richerol, T., Rochon, A., Blasco, S., Scott, D. B., Schell, T. M. and Bennett, R. J., 2008b. Evolution of paleo sea-surface conditions over the last 600 years in the Mackenzie Trough, Beaufort Sea (Canada). Marine Micropaleontology, 68, 6-20.
Richerol, T., Pienitz, R. and Rochon, A., 2012. Modern dinoflagellate cyst assemblages in surface sediments of Nunatsiavut fjords (Labrador, Canada). Marine Micropaleontology, 88-89, 54-64.
Richerol, T., Pienitz, R. and Rochon, A., 2014. Recent anthropogenic and climatic history of Nunatsiavut fjords (Labrador, Canada). Paleoceanography, DOI: 10.1002/2014PA002624.
Ritchie, J. C., 1987. Postglacial vegetation of Canada: 5. Eastern Canada – fossil record and reconstruction. Cambridge University Press.
Roberts, B. A., Simon, N. P. P. and K. W. Deering, 2006. The forest and woodlands of Labrador, Canada: ecology, distribution and future management. Ecological Research, 21, 868-880.
Rochon, A. and de Vernal, A., 1994. Palynomorph distribution in recent sediments from the Labrador Sea. Canadian Journal of Earth Sciences, 31, 115-127.
Rochon, A., de Vernal, A., Turon, J.-L., Matthiessen, J. and Head, M.J., 1999. Distribution of recent dinoflagellate cysts in surface sediments from the North Atlantic Ocean and

adjacent seas in relation to sea-surface parameters. Contribution Series Number 35, American Association of Stratigraphic Palynologists Foundation : Dallas, TX; 152pp.
Rousseau, C., 1974. Géographie floristique du Québec/Labrador – distribution des principales espèces vasculaires. Les Presses de l'Université Laval, Travaux et Documents du Centre d'Études Nordiques (CEN).
Saulnier-Talbot, E. and Pienitz, R., 2010. Postglacial chironomid assemblage succession in northernmost Ungava Peninsula, Canada. Journal of Quaternary Science, 25(2), 203-213.
Seidenkrantz, M.-S., Roncaglia, L., Fischel, A., Heilmann-Clausen, C., Kuijpers, A. and Moros, M., 2008. Variable North Atlantic climate seesaw patterns documented by a late Holocene marine record from Disko Bugt, West Greenland. Marine Micropaleontology, 68, 66-83.
Shaw, J., Gareau, P. and Courtney, R. C., 2002. Palaeogeography of Atlantic Canada 13-0 kyr. Quaternary Science Reviews, 21, 1861-1878.
Shaw, J., Piper, D. J. W., Fader, G. B. J., King, E. L., Todd, B. J., Bell. T., Batterson, M. J. and Liverman, D. G. E., 2006. A conceptual model of the deglaciation of Atlantic Canada. Quaternary Science Reviews, 25, 2059-2081.
Short, S. K. and Nichols, H., 1977. Holocene pollen diagrams from subarctic Labrador-Ungava : Vegetational history and climatic change. Arctic and Alpine Research, 9, 265-290.
Smol, J. P., Wolfe, A. P., Birks, H. J. B., Douglas, M. S. V., Jones, V. J., Korhola, A., Pienitz, R., Rühland, K., Sorvari, S., Antoniades, D., Brooks, S. J., Fallu, M.-A., Hughes, M., Keatley, B. E., Laing, T. E., Michelutti, N., Nazarova, L., Nyman, M., Paterson, A. M., Perren, B., Quinlan, R., Rautio, M., Saulnier-Talbot, E., Siitonen, S., Solovieva, N. and Weckström, J., 2005. Climate-driven regime shifts in the biological communities of arctic lakes. Presentation of the National Academy of Sciences of the USA, 102(12), 4397-4402.
Solignac, S., Seidenkrantz, M.-S., Jessen, C., Kuijpers, A., Gunvald, A. K. and Olsen, J., 2011. Late-Holocene sea-surface conditions offshore Newfoundland based on dinoflagellate cysts. The Holocene, 21(4), 539-552.
St-Onge, G., Leduc, J., Bilodeau, G., de Vernal, A., Devillers, R., Hillaire-Marcel, C., Loucheur, V., Marmen, S., Mucci, A. et Zhang, D., 1999. Caractérisation des sédiments récents du fjord du Saguenay (Québec) à partir de traceurs physiques, géochimiques, isotopiques et micropaléontologiques. Géographie Physique et Quaternaire, 53(3), 339-350.
Stuiver, M., Reimer, P. J. and Reimer, R. W., 2005. CALIB 7.0. http://calib.qub.ac.uk/calib/, last access 2013-09-30.
Ullah, W., Beersing, A., Blouin, A., Wood, C. H. and Rodgers, A., 1992. Water Resources Atlas of Newfoundland. Water Resources Division - Department of Environment and Lands - Government of Newfoudland and Labrador, pages ii-80.
Viau, A. E., Gajewski, K., Fines, P., Atkinson, D. E. and Sawada, M. C., 2002. Widespread evidence of 1500 yr climate variability in North America during the past 14 000 yr. Geology, 30(5),. 455-458.
Viau, A. E. and Gajewski, K., 2009. Reconstructing millennial-scale, regional paleoclimates of boreal Canada during the Holocene. Journal of Climate, 22(2), 316-320.
Vinther, B. M., Buchardt, S. L., Clausen, H. B., Dahl-Jensen, D., Johnsen, S. J., Fisher, D. A., Koerner, R. M., Raynaud, D., Lipenkov, V., Andersen, K. K., Blunier, T., Rasmussen, S. O., Steffensen, J. P. and Svensson, A. M., 2009. Holocene thinning of the Greenland ice sheet. Nature, 461, 385-388.

Whitmore, J., Gajewski, K., Sawada, M., Williams, J. W., Shuman, B., Bartlein, P. J., Minckley, T., Viau, A. E., Webb III, T., Shafer, S., Anderson, P. and Brubaker, L., 2005. Modern pollen data from North America and Greenland for multiscale paleoenvironmental applications. Quaternary Science Reviews, 24, 1828–1848.

Zonneveld, K. A. F., Versteegh, G. J. M. and de Lange, G. J., 1997. Preservation of organic-walled dinoflagellate cysts in different oxygen regimes: a 10,000 years natural experiment. Marine Micropaleontology, 29, 393-405.

Zonneveld, K. A. F. and Brummer, G.-J. A., 2000. (Palaeo-)ecological significance, transport and preservation of organic-walled dinoflagellate cysts in the Somali Basin, NW Arabian Sea. Deep-Sea Research II, 47, 2229-2256.

Zonneveld, K. A. F., Versteegh, G. J. M. and de Lange, G. J., 2001. Palaeoproductivity and post-depositional aerobic organic matter decay reflected by dinoflagellate cyst assemblages of the Eastern Mediterranean S1 sapropel. Marine Geology, 172, 181-195.